LASER
& PHOTONICS
REVIEWS

Supporting Information

for *Laser Photonics Rev.*, DOI 10.1002/lpor.202100457

Transverse-Electric-Polarized Polaritons Propagating in a $WS_2/Si_3N_4/Ag$ Heterostructure

*Shulei Li, Lidan Zhou, Fu Deng, Jin Xiang, Mingcheng Panmai, Hongxing Huang, Guangcan Li, Jingdong Chen and Sheng Lan**

Supporting Information

Transverse-electric polarized polaritons propagating in a $WS_2/Si_3N_4/Ag$ heterostructure

Shulei Li, Lidan Zhou, Fu Deng, Jin Xiang, Mingcheng Panmai, Hongxing Huang, Guangcan Li, Jingdong Chen and Sheng Lan*

Dr. Shulei Li, Ms. Lidan Zhou, Mr. Mingcheng Panmai, Mr. Hongxing Huang, Dr. Guangcan Li and Prof. Sheng Lan
Guangdong Provincial Key Laboratory of Nanophotonic Functional Materials and Devices, School of Information and Optoelectronic Science and Engineering
South China Normal University
Guangzhou 510006, P. R. China
slan@scnu.edu.cn (S. Lan)

Dr. Shulei Li,
School of Optoelectronic Engineering
Guangdong Polytechnic Normal University
Guangzhou 510665, P. R. China

Mr. Fu Deng
Department of Physics
The Hong Kong University of Science and Technology
Hong Kong, P. R. China

Dr. Jin Xiang
Key Laboratory of Optoelectronic Technology and Systems (Chongqing University), Ministry of Education, School of Optoelectronic Engineering
Chongqing University
Chongqing 400044, P. R. China

Dr. Jingdong Chen
College of Physics and Information Engineering
Minnan Normal University
Zhangzhou 363000, P. R. China

Supplementary Note 1: Electric field distribution and enhancement in a thin dielectric film

In this work, the strong localization of the electric field of the transverse-electric (TE) wave supported by a Si_3N_4/Ag heterostructure is employed to realize strong coupling simultaneously with the two exciton resonances of WS_2 monolayer. Here, the thin Ag film plays a crucial role for the excitation of the TE wave whose electric field is localized on the surface of the Si_3N_4 film. For comparison, we also calculated the electric field distributions in a thin Si_3N_4 film with a thickness of d = 50 nm for two perpendicular polarizations, as shown in Figure S1. For a transverse-magnetic (TM) wave, the electric field is distributed outside the Si_3N_4 film. Moreover, it is dominated by the component perpendicular to the Si_3N_4 film (i.e., E_y ~0) which is not suitable for the coupling with the excitons in WS_2 monolayer. For a TE wave whose electric field is parallel to the dielectric film (E_y), the electric field is localized inside the Si_3N_4 film (not on the surface). The enhancement factor on the surface of the Si_3N_4 film is quite small (~1.8).

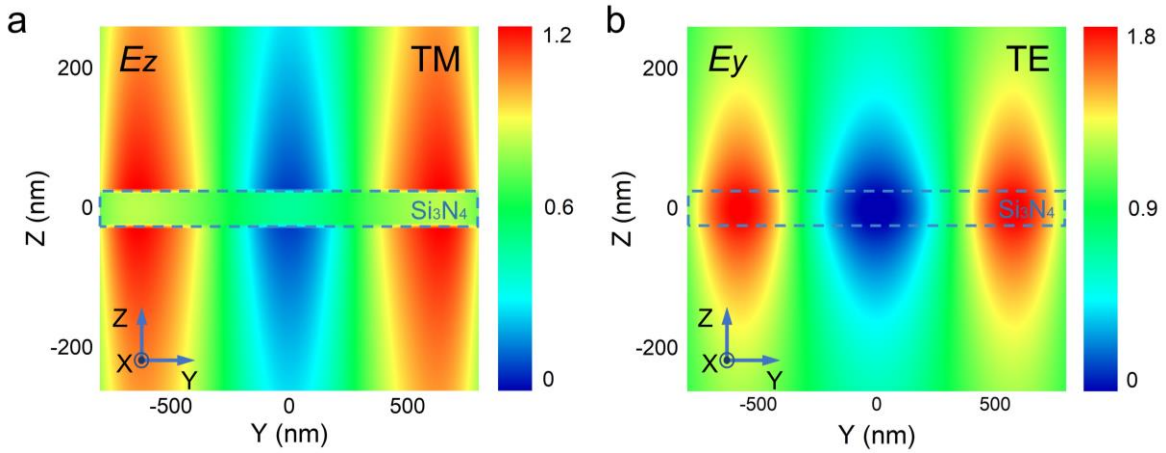

Figure S1. Electric field distributions in a S_3N_4 film with d = 50 nm calculated for a) TM and b) TE waves at 500 nm.

Supplementary Note 2: Optical properties of a Si_3N_4/Ag heterostructures with different thicknesses of Si_3N_4 layer

In Figure S2a, we show the resonant energies of the TE waves of different orders calculated for Si_3N_4/Ag heterostructures composed of Si_3N_4 layers with different thicknesses. The incidence angle is fixed at θ = 45°. In Figure S2b, we present the reflection spectra simulated for Si_3N_4/Ag heterostructures composed of Si_3N_4 layers with different thicknesses. Apparently, the reflection dip representing the resonant energy of the TE wave is redshifted from 2.79 to 2.48 eV when the thickness of the Si_3N_4 is increased from 45 to 55 nm. In practice, this feature of the TE wave can be exploited to build highly sensitive optical sensors.

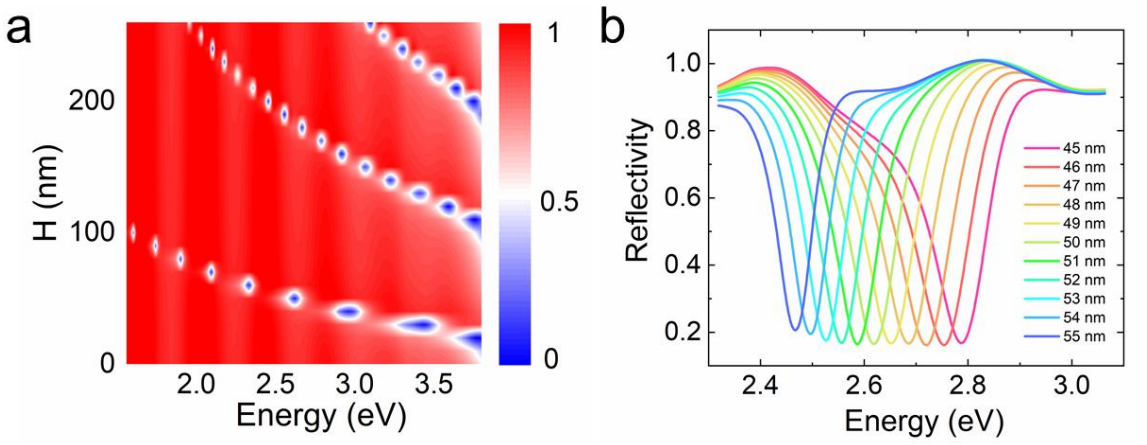

Figure S2. a) Resonant energies of the TE waves of different orders excited in Si_3N_4/Ag heterostructures composed of Si_3N_4 layers with different thicknesses. b) Reflection spectra calculated for Si_3N_4/Ag heterostructures composed of Si_3N_4 layers with different thicknesses.

Supplementary Note 3: Dispersion relations of the TM and TE waves supported by a S_3N_4/Ag heterostructure

The TE waves supported by a Si_3N_4/Ag heterostructure belong to waveguide modes which can only be excited by using evanescent wave. In Figure S3, we show the dispersion relation of the lowest order TE wave supported by a Si_3N_4/Ag with d = 100 nm. The dispersion relation of the lowest order TM wave is also provided for comparison. It is noticed that both dispersion relations are located under the light line, implying that both TE and TM waves can only be excited by using evanescent wave.

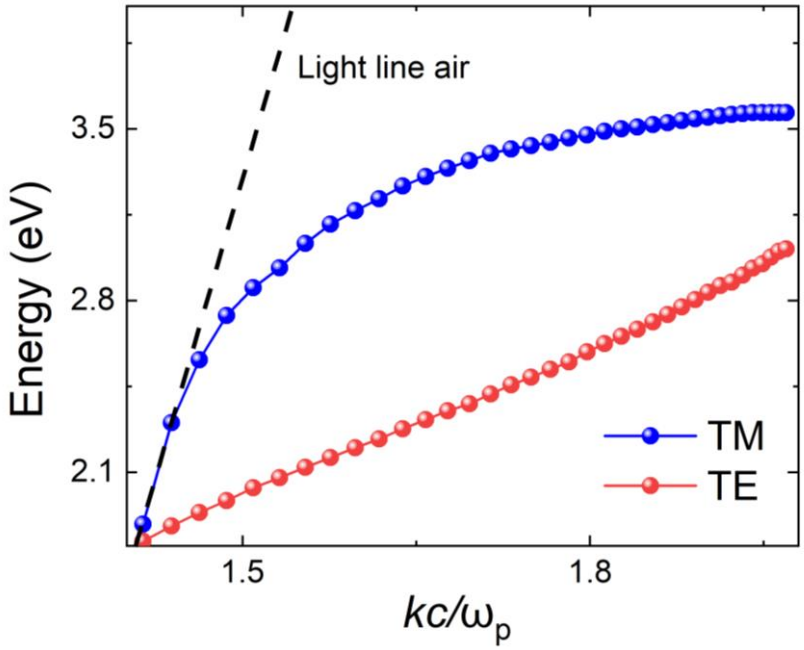

Figure S3. Dispersion relations of the lowest order TM and TE waves supported by a Si_3N_4/Ag heterostructure with d = 100 nm.

Supplementary Note 4: Optical properties of TE waves excited in Si_3N_4/Ag heterostructures

As discussed in the main text, the spatial separation of electric and magnetic fields in a TE wave is responsible for the large quality factor or the narrow linewidth. Since a TE wave supported by a dielectric-metal heterostructure can only be excited by using the total internal reflection configuration, it can be considered as a "dark" mode with negligible radiation loss. It can be perfectly extracted by using a scatter placed on the dielectric layer. In Figure S4, we present the frequency spectrum of the lowest-order TE wave excited in a Si_3N_4/Ag heterostructure and extracted by using a polystyrene (PS) nanoparticle with a diameter of 300 nm. The radiation spectrum of the TE wave propagating in the heterostructure is also provided for comparison. Since the electric field of a TE wave is mainly localized on the surface of the dielectric layer, the propagation loss of the TE wave comes mainly from the extension of the electric field into the metal film.

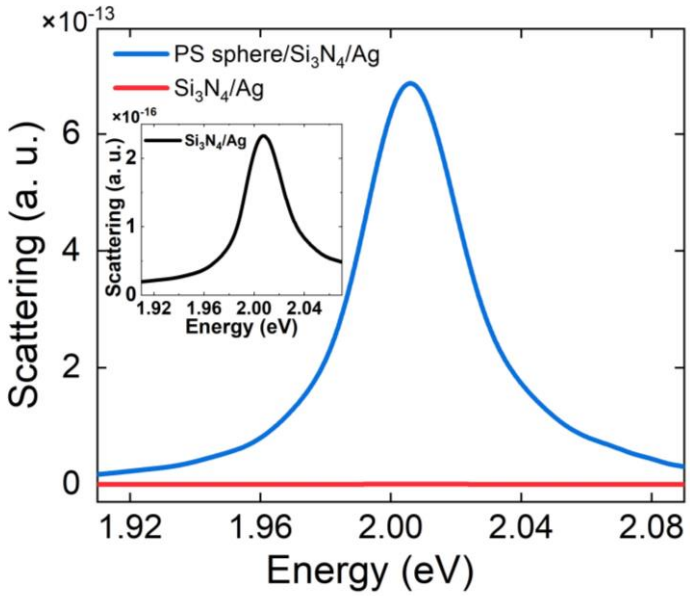

Figure S4. Scattering spectrum of the PS nanoparticle with a diameter of 300 nm excited by using the TE wave supported by a Si_3N_4/Ag heterostructure. The radiation spectrum of the TE wave in the absence of the PS nanoparticle is also provided for comparison.

Supplementary Note 5: Electric and magnetic field distributions for the TM and TE waves

We compare the electric and magnetic field distributions of the TM wave (i.e., the SPPs) excited on the surface of a bare Ag film with those of the TE wave excited in a Si_3N_4/Ag heterostructure. The TM and TE waves were excited by using p- and s-polarized white light with an incidence angle of $\theta = 48°$ respectively. The corresponding electric and magnetic field distributions are shown in Figure S5a,b and Figure S5c,d, respectively. For the TE wave, it is remarkable that the in-plane electric field (E_y) is localized on the surface of the Si_3N_4 layer while the magnetic field (H_x) is localized at the interface between the Si_3N_4 layer and the Ag film for the TE wave. This behavior is completely different from that observed for the TM wave for which both the electric and magnetic fields are localized on the surface of the Ag film. We inspect the in-plane electric field (E_y), which is crucial for the coupling of the TE wave with the excitons in the two-dimensional material. It is found that the enhancement factor is larger than that observed for the TM wave by a factor of ~3.0.

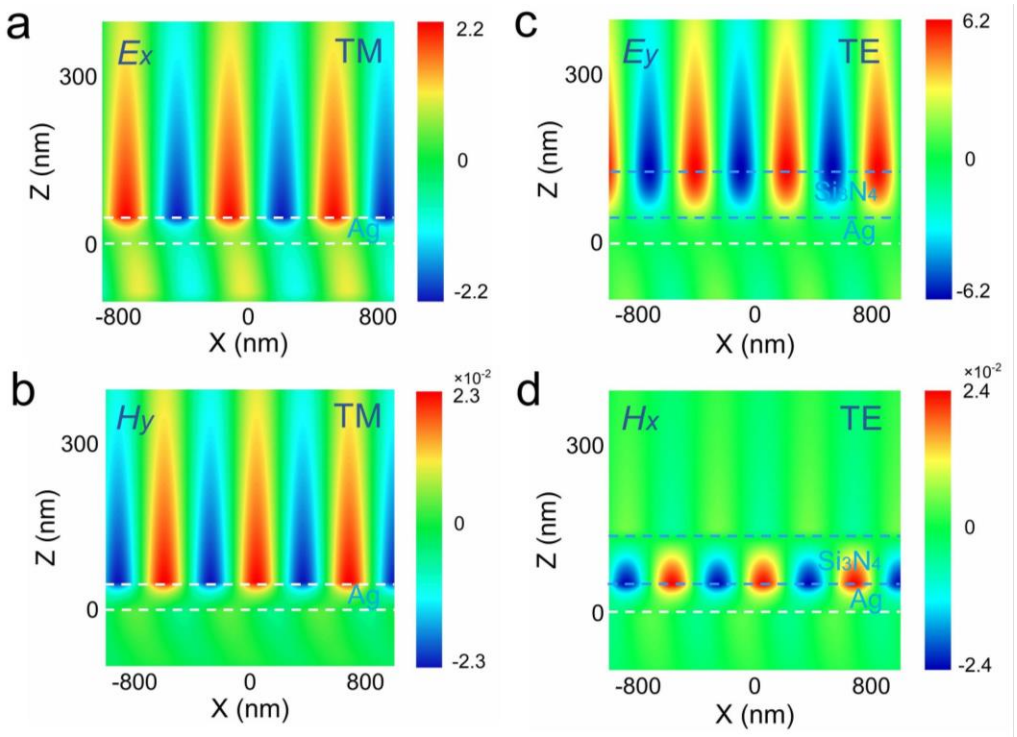

Figure S5. The in-plane electric and magnetic field distributions in the XZ plane calculated for the TM (a,b) and TE (c,d) waves.

Supplementary Note 6: Critical coupling strength at the quantum exceptional point

Basically, the eigen-energies of the hybrid states (E_+ and E_-) originating from the coupling between the TE wave and the exciton resonance can be calculated by using Eq. (2). In Figure S6a, we show the depedence of the eigen-energies of the hybrid states (E_+ and E_-) on the coupling strength (g) between the TE wave and the exciton resonance of WS_2 monolayer. Here, the enerygies of the TE wave and the exciton resonance are assumed to be the same ($E_{TE} = E_{ex} = 2.02$ eV). We examine three cases in which the damping rates of the TE wave and the exciton resonance are intentionally chosen to be different. The average dampling rate of the TE wave and the exciton resonance is kept as a constant (i.e., $(\gamma_{TE}+\gamma_{ex})/2 = 30$ meV). It is noticed that the splitting of the hybrid states occurs at the so-called quantum exceptional point where the coupling strength g_{QEP} is defined by Eq. (4). The manimum $g_{QEP} = 0$ is achieved when the damping rates of the TE wave and the exciton resonance becomes equal (i.e., $\gamma_{TE} = \gamma_{ex} = 30$ meV). For a specific coupling stength g, the largest energy spliiting ($E_+ - E_- = \hbar\Omega$) is obtained in the case of $g_{QEP} = 0$. If we consider the coupling strength (g_{strong}) where the strong coupling criterion is fullfilled (see Eq. (5)), it is found that the smallest $g_{strong} = 15.0$ meV is also observed in the case of $g_{QEP} = 0$. In Figure S6b, we present the calculation results for another three cases in which the damping rate of the exciton resonance is fixed ($\gamma_{ex} = 30$ meV) while that of the TE wave is varaible. Similarly, the smallest coupling strength for realizing strong coupling is also observed in the case of $g_{QEP} = 0$ ($g_{strong} = 15.0$ meV). Therefore, it indicates that a coupling system with a small g_{QEP} can be considered as an advantage for realizing strong coupling, as described in the main text.

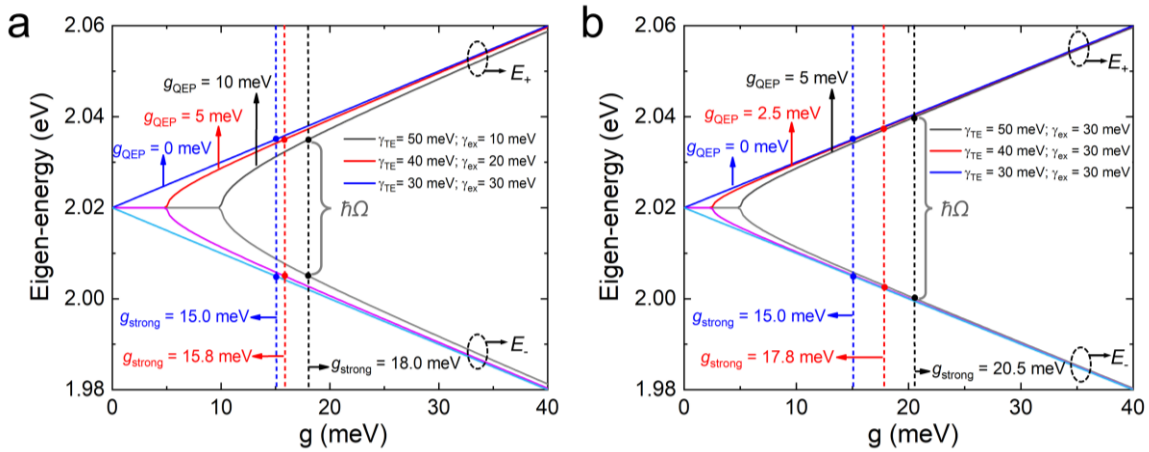

Figure S6. a) Depedence of the eigen-energies of the hybrid states (E_+ and E_-) on the coupling strength (g) between the TE wave and the exciton resonance of WS_2 monolayer. In this case, the average damping rate of the TE wave and the excition resonance is kept as a constant (i.e., $(\gamma_{TE}+\gamma_{ex})/2 = 30$ meV). b) Depedence of the eigen-energies of the hybrid states (E_+ and E_-) on the coupling strength (g) between the TE wave and the exciton

resonance of WS_2 monolayer. In this case, the damping rate of the exciton resonance is fixed (γ_{ex} = 30 meV) while that of the TE wave is varaible.

Supplementary Note 7: Coupling of TE wave and X_A exciton in Si_3N_4/WS_2/Ag heterostructures

As mentioned above, the electric field of the TE wave supported in a Si_3N_4 layer is strongly localized on the surface of the Si_3N_4 layer while the magnetic field is localized at the interface between the Si_3N_4 layer and the Ag film. Now we inserted a WS_2 monolayer in between the Si_3N_4 layer and the Ag film and examined the coupling between the TE wave and the A excitons in the WS_2 monolayer. The resonant wavelength of the TE wave was adjusted across the exciton resonance by varying the incidence angle of the excitation white light. The reflection spectra obtained at different incidence angles are shown in Figure S7. A small energy splitting of ~41 meV was observed when the TE wave is tuned to be resonant with the exciton resonance, The energy splitting is induced by the in-plane electric field of the TE wave which is attenuated from the surface of the Si_3N_4 layer.

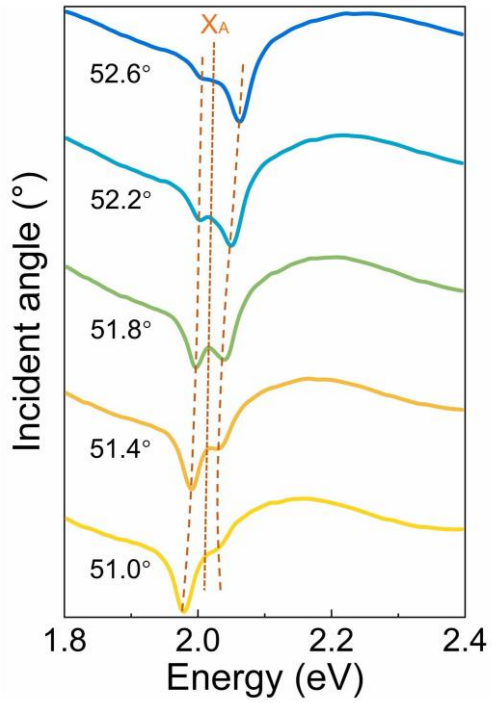

Figure S7. Reflection spectra calculated for the Si_3N_4/WS_2/Ag heterostructure at different incidence angles.

Supplementary Note 8: Coupling of TM wave and the excitons in WS_2 monolayer

By placing a two-dimensional material (e.g., a WS_2 monolayer) on a thin metal (e.g., Ag) film, one can reveal an anti-crossing behavior in the angle-resolved reflection spectra of the p-polarized white light, implying the extitence of plasmon-exciton coupling, as shown in Figure S8a. The values of energy splitting at the two exciton resonances of the WS_2 monolayer can be derived from the reflection spectra obtained at θ = 45.8° and 47.4°, respectively, where the intensities of the two reflection dips are equal, as shown in Figure S8b. They were found to be $\hbar\Omega_A$ = 89.8 meV and $\hbar\Omega_B$ = 82.9 meV. Here, we employed a classical coupled harmonic oscillator model to characterize the plasmon-exciton coupling strength. The linewidths of the X_A and X_B exciton resonances are 33 and 80 meV while the linewidths of the TM waves at the same wavelength are 190 and 230 meV, respectively. The criterion for strong coupling, which is $\hbar\Omega > |\gamma_{TE} \pm \gamma_{ex}|/2$, is satisfied for both excitons, implying that the plasmon-exciton coupling for the two excitons (X_A and X_B) enters into the strong coupling regime although the enhancement factor for the in-plane electric field (E_x) is not large (~2.2).

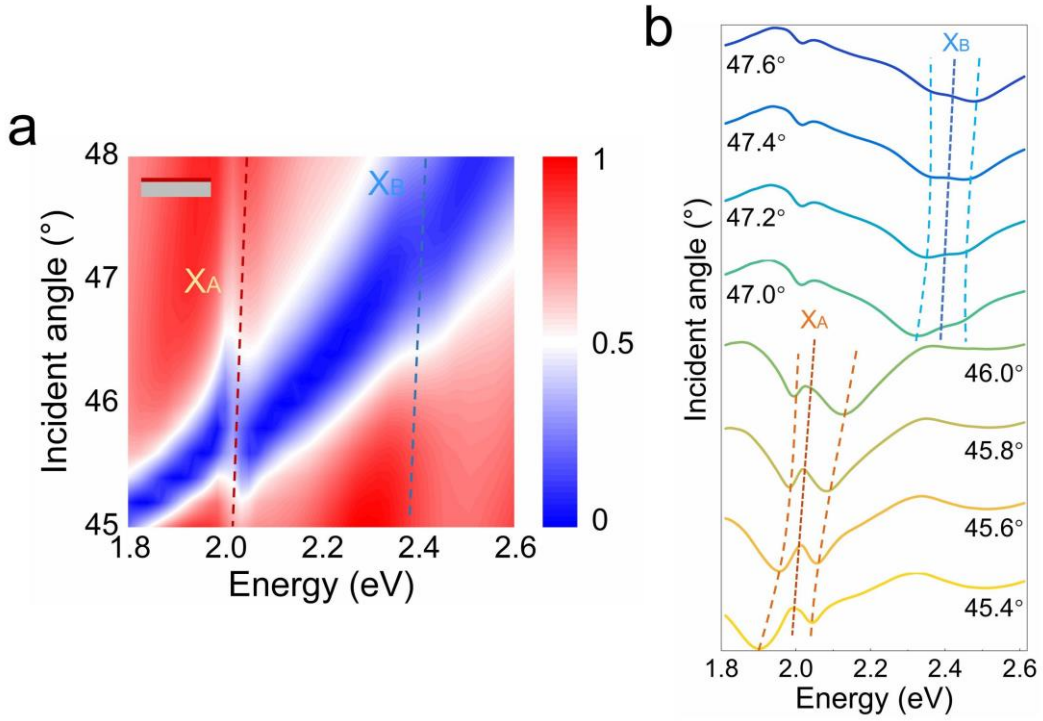

Figure S8. a) Angle-resolved reflection spectra calculated for a WS_2/Ag heterostructure by using a *p*-polarized white light. b) Reflection spectra calculated for the WS_2/Ag heterostructure at different incidence angles.

Supplementary Note 9: Electric and magnetic field distributions calculated for a PS nanoparticle placed on a Si_3N_4/Ag heterostructure

Instead of measuring the reflection spectra of a Si_3N_4/Ag heterostructure, which is not convenient from the experiment point of view, we characterized the optical properties of the TE waves by examining the scattering spectra of a PS nanoparticle placed on the Si_3N_4 layer. For this reason, we simulated the in-plane electric and magnetic field distributions for a PS nanoparticle with a diameter of d = 300 nm located on the Si_3N_4/Ag heterostructure at the two incidence angles (50° and 60°), which was used to scatter the TE wave excited in the heterostructure, as shown in Figure S9. It is noticed that the in-plane electric field is enhanced in both cases at the location of the PS nanoparticle.

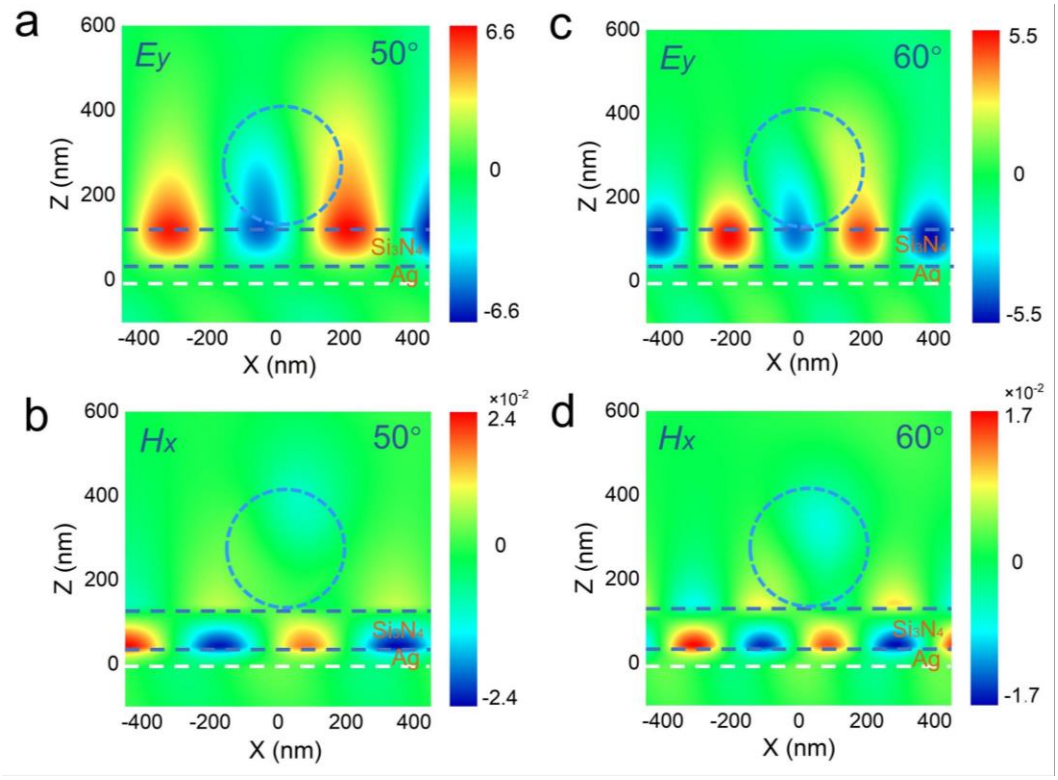

Figure S9. Electric and magnetic field distributions in the XZ plane calculated for a PS nanoparticle with d = 300 nm located on the Si_3N_4/Ag heterostructure. a,b) The E_y and H_x components for the TE wave at an incidence angle of 50°. c,d) The E_y and H_x components for the TE wave at an incidence angle of 60°.

Supplementary Note 10: Electric and magnetic field distributions calculated for a PS nanoparticle placed on a $WS_2/Si_3N_4/Ag$ heterostructure

We examined the in-plane electric field distributions calculated for a PS nanoparticle placed on a $WS_2/Si_3N_4/Ag$ heterostructure and excited by using s-polarized white light with different incidence angles, as shown in Figure S10. When the TE wave approaches the exciton resonance from the low energy side, one can see a reduction of the electric field and a broadening of the linewidth, as shown in Figure S10a,b, where the electric field distributions calculated at θ = 50° and 51° are presented. A significant attenuation of the electric field is observed when the TE wave is moved to the high-energy side of the exciton resonance, as shown in Figure S10d, where the electric field distribution calculated at θ = 53° is shown. It indicates that the energy of the system, which is initially stored in the TE wave in the lower branch, has been transferred to the excitons of the WS_2 monolayer in the upper branch.

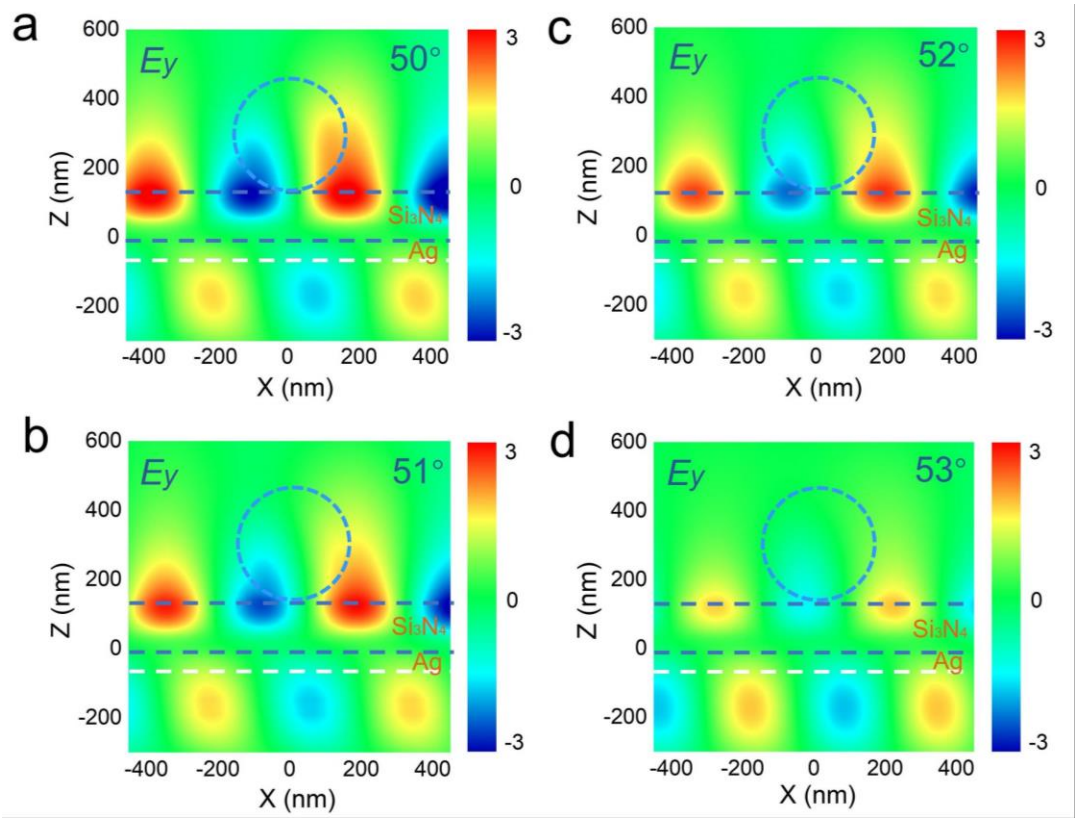

Figure S10. In–palne electric field (*Ey*) in the XZ plane calculated for a PS nanoparticle excited by the TE wave at different incidence angles of a) 50°, b) 51°, c) 52°, d) 53°.